LAWRENCE
LIVERMORE
NATIONAL
LABORATORY

Progress with the COGENT Edge Kinetic Code: CollisionOperator Options

M. Dorf, R. H. Cohen, J. C. Compton, M. Dorr, T. D. Rognlien, J. Angus, S. Krasheninnikov, P. Colella, D. Martin, P. McCorquodale

September 14, 2011

Disclaimer

This document was prepared as an account of work sponsored by an agency of the United States government. Neither the United States government nor Lawrence Livermore National Security, LLC, nor any of their employees makes any warranty, expressed or implied, or assumes any legal liability or responsibility for the accuracy, completeness, or usefulness of any information, apparatus, product, or process disclosed, or represents that its use would not infringe privately owned rights. Reference herein to any specific commercial product, process, or service by trade name, trademark, manufacturer, or otherwise does not necessarily constitute or imply its endorsement, recommendation, or favoring by the United States government or Lawrence Livermore National Security, LLC. The views and opinions of authors expressed herein do not necessarily state or reflect those of the United States government or Lawrence Livermore National Security, LLC, and shall not be used for advertising or product endorsement purposes.

Progress with the COGENT Edge Kinetic Code: Collision Operator Options

M. A. Dorf[*][1], **R. H. Cohen**[1], **J. C. Compton**[1], **M. Dorr**[1], **T. D. Rognlien**[1], **J. Angus**[2], **S. Krasheninnikov**[2], **P. Colella**[3], **D. Martin**[3], and **P. McCorquodale**[3]

[1] Lawrence Livermore National Laboratory, Livermore, CA 94550 USA
[2] University of California, San Diego, La Jolla, CA 92093 USA
[3] Lawrence Berkeley National Laboratory, Berkeley, CA 94720 USA

COGENT is a continuum gyrokinetic code for edge plasmas being developed by the Edge Simulation Laboratory collaboration. The code is distinguished by application of the fourth order conservative discretization, and mapped multiblock grid technology to handle the geometric complexity of the tokamak edge. It is written in $v_\parallel$ - μ (parallel velocity – magnetic moment) velocity coordinates, and making use of the gyrokinetic Poisson equation for the calculation of a self-consistent electric potential. In the present manuscript we report on the implementation and initial testing of a succession of increasingly detailed collision operator options, including a simple drag-diffusion operator in the parallel velocity space, Lorentz collisions, and a linearized model Fokker-Planck collision operator conserving momentum and energy.

1   Introduction

Although δf particle-in-cell (PIC) simulation techniques available for modeling of the tokamak core region can provide low level of numerical noise, concern about PIC noise in the full-f simulations required to model large density variations in the tokamak edge motivates the use of a continuum kinetic code for the edge modeling [1]. Making use of advanced numerical methods from fluids community, and building on the success of continuum core codes [1] (e.g., GYRO, GENE, etc.) and the continuum edge code TEMPEST [1, 2], the Edge Simulation Laboratory collaboration (ESL) has started development of a new-generation continuum kinetic code COGENT. The COGENT code solves the conservative form of the gyro-kinetic equations by making use of the fourth-order finite-volume (conservative) discretization independent of grid choice, hence providing no loss of accuracy order in going to non-uniform grid [3, 4]. This framework allows using arbitrary mapped multiblock grids (field-aligned on blocks) to handle the complexity of divertor geometry without loss of accuracy. Another distinguishing feature of the code is the use of the Colella-Sekora flux-limiter to suppress unphysical oscillations about discontinuities while maintaining high-order accuracy elsewhere [5]. Finally, the code is written in $v_\parallel$-μ (parallel velocity – magnetic moment) coordinates, which avoids "cut-cell" issues appearing, for instance, when E - μ (energy – magnetic moment) coordinates are used.

The performance of the numerical algorithms utilized for solving the gyrokinetic Vlasov-Poisson equations has been successfully tested in the simulation of the collisionless relaxation of geodesic acoustic modes (GAMs), and an excellent agreement with an analytical theory along with 4-order convergence of the numerical errors have been observed [4]. In the present work the report on implementation and testing of a succession of increasingly detailed collision operator options, including a simple drag-diffusion operator in the parallel velocity space, Lorentz collisions, and a linearized model Fokker-Planck collision operator conserving momentum and

[*]   Corresponding author: e-mail: dorf1@llnl.gov, Phone: +1 925 422 5181, Fax: +1 925 423 3484

energy. Finally, we note that we have also implemented and tested the Krook collision model, however, for brevity, we do not report the results of those studies in the present work.

2   Simulation model

The present 4D version of the COGENT code (2 configuration space + 2 velocity space coordinates) solves axisymmetric electrostatic multi-species gyrokinetic Boltzman-Poisson equations for the gyrocenter distribution functions $f_\alpha(\mathbf{R}, v_\parallel, \mu, t)$ and the electrostatic potential $\Phi(\mathbf{R}, t)$. Here $\mathbf{R}$ is the gyrocenter position coordinate, $v_\parallel$ is the parallel velocity, μ is the magnetic moment, and the corresponding kinetic equation is given by [6]

$$\frac{\partial f_\alpha}{\partial t} + \frac{d\mathbf{R}_\alpha}{dt} \nabla f_\alpha + \frac{dv_{\parallel\alpha}}{dt} \frac{\partial f_\alpha}{\partial v_\parallel} = C_\alpha[f_\alpha], \tag{1}$$

where $d\mathbf{R}/dt = \mathbf{V}_{gc} = v_\parallel \mathbf{b} + \mathbf{V}_{dr}$ and $dv_{\parallel\alpha}/dt = (-1/m_\alpha v_{\parallel\alpha})\mathbf{V}_{gc} \cdot (Z_\alpha \nabla \Phi + \mu \nabla B)$, $\mathbf{V}_{dr}$ is the magnetic drift velocity composed of the E×B drift, curvature drift, and ∇B drift [6], $\mathbf{B}$ is the applied magnetic field, and $C_\alpha[f_\alpha]$ is the collision operator. The present version of the code assumes the long wavelength limit $k_\perp \rho_\alpha \ll 1$, in which the gyrokinetic Poisson equation takes the form [1, 7]

$$\Delta^2 \Phi = 4\pi e \left(n_e - \sum_\alpha n_{\alpha, gc} \right) - 4\pi e^2 \sum_\alpha \frac{Z_\alpha}{m_\alpha \Omega_\alpha^2} \nabla_\perp \cdot \left(n_{\alpha, gc} \nabla_\perp \Phi \right). \tag{2}$$

Here, $n_{\alpha, gc} = (2\pi/m_\alpha) \int B^*_{\parallel\alpha} dv_\parallel d\mu \{ f_\alpha + (\rho_\alpha^2/2) \nabla_\perp^2 f_\alpha \}$ is the ion gyrocenter density, $B^*_{\parallel\alpha} = B[1 + (v_\parallel/\Omega_\alpha)\mathbf{b} \cdot \nabla \times \mathbf{b}]$, Ω_α and ρ_α denote the species cyclotron frequency and thermal gyroradius, and various adiabatic models are available in the code to model the electron density, n_e.

3   Collision models

Several model collision operators have been implemented and tested in COGENT. These include a model parallel drag-diffusion collision operator, the Lorentz operator, and the linearized Fokker-Plank collision operator in the form proposed by Abel et al in Ref. [8]. In what follows, a brief description of collision models along with the summary of initial tests is presented.

3.1 Parallel drag-diffusion collision operator

A model "parallel drag-diffusion" operator

$$C_\parallel = v_c \partial_{v_\parallel} \left(v_\parallel f + (T/m) \partial_{v_\parallel} f \right) \tag{3}$$

provides drag and diffusion in the parallel velocity space. Here, v_c is the collision frequency, the derivative with respect to the parallel velocity coordinate, $\partial_{v_\parallel} \equiv \partial/\partial v_\parallel$, is evaluated at a fixed magnetic moment, and m and T correspond to the species mass and equilibrium temperature, respectively. The implementation of this collision model has been verified for a test problem, where particles confined along the magnetic field direction by a square electrostatic potential well become untrapped due to collisions and are lost. A schematic of the simulation domain is shown in Fig. 1(a). For this simulation the magnetic drifts are turned off, and only the parallel streaming is allowed. The potential distribution shown in Fig. 1(b) is effectively modeled by the corresponding boundary conditions at $\theta = 0$ ($\theta = 2\pi$) plane, which provide reflection of low-energy incident particles with $v_\parallel < (2q\varphi_0/m)^{1/2}$ and absorption of high-energy particles with $v_\parallel > (2q\varphi_0/m)^{1/2}$. Here, q is the particle charge, and φ_0 is the magnitude of the potential barrier. The simulation is initialized with a uniform Maxwellian distribution function $f_M = (1/\pi v_T)^{3/2} n_0 \exp(-v^2/v_T^2 - \mu B/T)$, where $v_T = (2T/m)^{1/2}$ is the thermal velocity.

An approximate analytical solution to the problem can be obtained in the weak-collision limit, i.e., for the case where the collision frequency, v_c, is much smaller than the effective bounce frequency, $\omega_B = v_T/2L_c$. Here, L_c is the connection length given for the present geometry by $L_c = (B/B_p) \cdot 2\pi r$, where B_p is the poloidal component of the applied magnetic field [Fig. 1(a)]. For this case the high-energy particles forming the tail of the initial
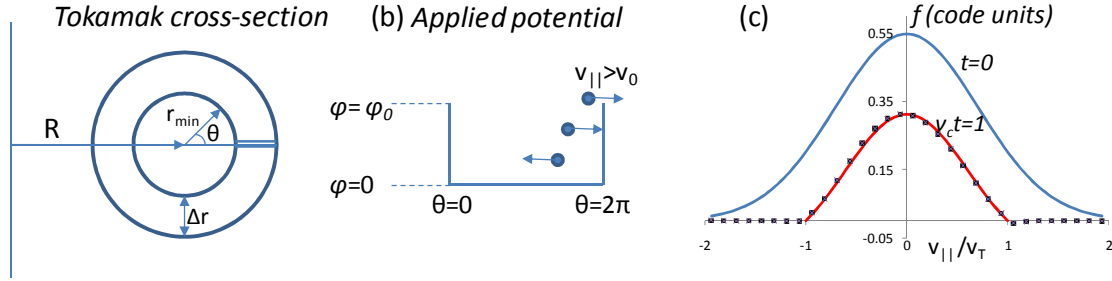
Fig. 1 Parallel particles losses over a potential barrier. (a) Schematic of the simulation geometry, r_{min}/R=0.0002, $\Delta r/r_{min}$=0.2, the ratio of the toroidal to the poloidal magnetic field is B_T/B_p=4. (b) Distribution of the applied potential. (c) Evolution of the particle distribution function in the weak-collision limit, ω_B/v_c=30, v_0=v_T. The black dots correspond to the results of the COGENT simulations, and the red curve shows the analytical solution given in Eq. (6), where C_0 is chosen to match the maximum value of the distribution function at t=1/v_c. Grid resolution corresponds to n_r=8, n_θ=32, $n_{v\parallel}$=32, n_μ=8.

distribution are rapidly lost on the time sale $\tau=L_c/v_0$, and during the following stage of a slow collisional decay the distribution function can be approximated by its bounce-average value F, which evolves according to

$$\partial F/\partial t = C_\parallel[F],\qquad(4)$$

Furthermore, in the weak-collision limit, i.e., $v_c \ll \Omega_B$, we can take (to the zero order in v_c/Ω_B) F=0 for $|v_\parallel|\geq v_0$. Equation (4) has a series of exact solutions

$$F_n(v_\parallel,\mu,t)= e^{-\lambda_n v_c t}e^{-v_\parallel^2/v_T^2}M\left[\lambda_n/2,1/2,v_\parallel^2/v_T^2\right]e^{-\mu B/T},\qquad(5)$$

where $M[a,b,x]$ is the Kummer confluent hypergeometric function, and the eigenvalues λ_n are determined from the boundary conditions $F(\pm v_0,\mu,t)$=0. The bounce-averaged distribution function can be now constructed as $F=\Sigma C_n F_n$, where the coefficients C_n are determined from the initial conditions. Note that for the considered parameters, v_0/v_T=1.0, the eigenvalues λ_n rapidly increase (λ_0=0.79, λ_1=10.75, λ_2=30.5 …), therefore after a relatively short transient time period, $\tau_{tr}\sim1/(v_c\lambda_1)$ the asymptotic behavior of the distribution function F, is given by

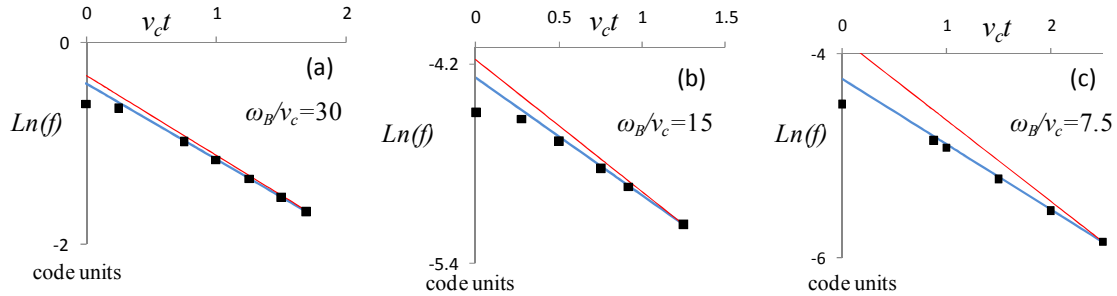$$F(v_\parallel,\mu,t \gg \tau_{tr})\cong C_0 F_0(v_\parallel,\mu,t)\qquad(6)$$

Fig. 2 Effects of finite v_c/ω_B corrections on the distribution function decay rate. Shown is the time evolution of the distribution function maximum value. The black dots correspond to the results of the COGENT simulations, the red lines show the weak-collision theoretical prediction, and the blue lines correspond to the decay rate obtained from the "sum rule" [Eq. (7)], where, for the considered parameters, γ_f=0.43ω_B.

Results of the numerical simulations obtained in the weak collision limit for ω_B/v_c=30 demonstrate excellent agreement with the analytical predictions [see Figs. 1(c) and 2(a)]. It is also interesting to note that the departure from the weak-collision decay rate observed in the simulations with an increased collision frequency [Figs. 2(b) and (c)] can be described well by the "sum rule" [9],

$$1/\gamma = 1/\gamma_c + 1/\gamma_f, \tag{7}$$

where, $\gamma=(1/N)dN/dt$ is the decay rate, N is the total number of particle, γ_c is the decay rate corresponding to the weak-collision limit ($\nu_c \ll \omega_B$), and γ_f is the decay rate corresponding to the strong-collision limit ($\nu_c \gg \omega_B$), in which the distribution function can be approximated by a Maxwellian distribution and the particle parallel losses are determined by the "gas-dynamic" flow, i.e.

$$\gamma_f = \frac{2}{L_\parallel} \int_{v_0}^\infty f_M v_\parallel dv_\parallel \bigg/ \int_{-\infty}^\infty f_M dv_\parallel = \frac{v_T}{\sqrt{\pi} L_\parallel} e^{-v_0^2/v_T^2} \tag{8}$$

Here, $L_\parallel$ is the parallel length of an electrostatic trap, given for the present geometry by $L_\parallel = L_c = (B/B_p) \cdot 2\pi r$.

3.2   Lorentz collision operator

The Lorentz operator,

$$C_L[f(\xi,v)] = \nu_c \frac{1}{2} \partial_\xi \left(\left(1 - \xi^2\right) \partial_\xi f \right) \tag{9}$$

provides pitch angle scattering in the velocity space. Here, ν_c is the collision frequency, the derivative with respect to the pitch-angle variable, $\xi = v_\parallel/v$, is evaluated at a fixed particle energy, $E = mv^2/2$, and a gyrophase-independent distribution function is assumed. Note that although the Lorentz operator conserves particles energy analytically, spurious diffusion in the energy space appears (see Fig. 3) due to approximate (finite-difference) numerical evaluation of the operator, using the parallel velocity $v_\parallel$ and magnetic moment μ coordinates. Therefore, it is of particular importance to develop and implement a higher-order finite-difference scheme that can minimize the effects of spurious energy diffusion. Figure 3 demonstrates that the spurious diffusion is significantly suppressed (to a tolerable level) for the case where a 4-th order accurate numerical scheme is implemented. In order to test the performance of the implemented Lorentz operator, full-f simulations of neoclassical transport have been performed. The results are found in very good agreement with the analytical theory developed in [10] for the case of the Lorentz operator (see Fig. 4).
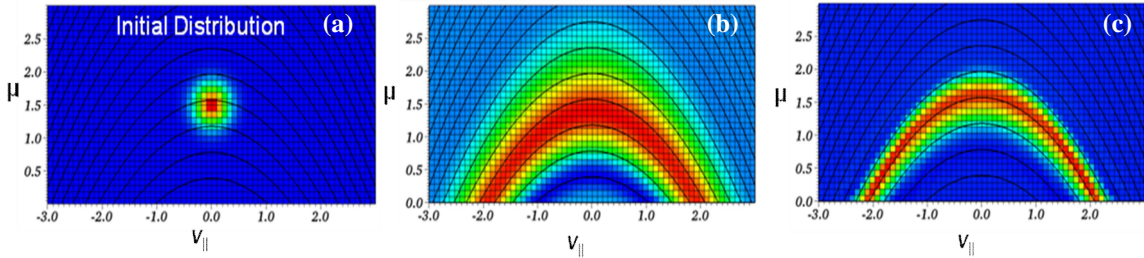

Fig. 3   COGENT simulations of the pitch-angle scattering of an initial distribution function represented by a blob in the velocity space. The figure shows plots of (a) the initial distribution (t=0), (b) distribution function at $\nu_c t=4$ obtained with the second-order accurate implementation of the Lorentz operator, and (c) distribution function at $\nu_c t=4$ obtained with the fourth-order accurate implementation of the Lorentz operator. The solid black lines illustrate the contours of constant energy. Note that the different scales in color schemes are used in the frames, and the maximum values of the distribution functions in frames (a), (b), and (c) are related as 1:0.067:0.13, correspondingly. Grid resolution in the velocity space corresponds to $n_{v_\parallel}=64$, $n_\mu=32$.

3.3   Full linearized collision operator and a simplified non-linear isotropic collision model

For brevity, we only mention here that a linearized model Fokker-Plank collision operator conserving momentum and energy has been recently implemented in COGENT in the form proposed by Abel et al in Ref. [8]. Also, a simplified nonlinear collision model taking into account isotropic nonthermal effects has been formulated by straightforward generalization of the linearized model. The nonlinear model operator for like-particle collisions takes the form
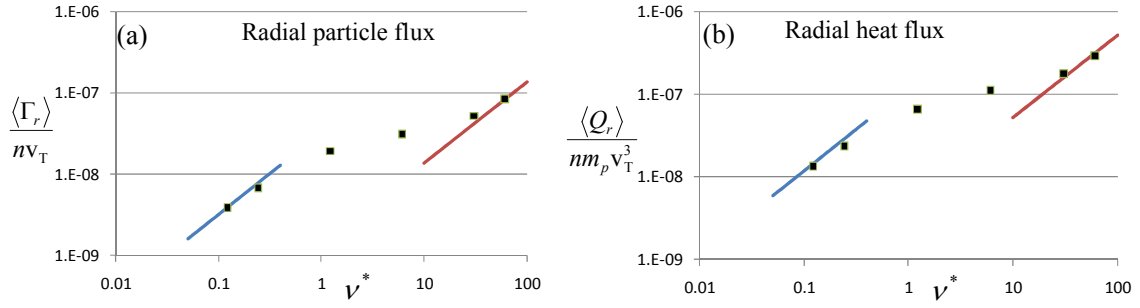
Fig. 4 COGENT simulations (dots) of the radial neoclassical ion transport for the case of the Lorentz collision operator. Shown the plots of (a) flux-surface averaged particle flux, and (b) flux-surface averaged heat flux versus the normalized collision frequency $\nu^* = \nu_c \varepsilon^{-3/2} 2^{1/2} q R_0 / v_T$. The red and blue lines correspond to the analytical calculations [10] in the banana and Pfirsch-Schluter regimes, correspondingly. The parameters of the simulation correspond to safety factor q=3, inverse aspect ratio ε=0.1, ion temperature T=3 KeV, ion mass m_i=2m_p, where m_p is the proton mass, major radius R_0=45.6 m, toroidal magnetic field on axis B_0=7.5T, inverse temperature and density gradients $\kappa_n = \kappa_T = 10/R_0$, and the magnetic field geometry corresponds to flux tubes with nested circular cross-sections. Grid resolution in [r, θ, $v_\parallel$, μ] domain corresponds to [16, 32, 80, 40] for the banana regime, and [16, 32, 32, 16] for the Pfirsch-Schluter regime.

$$C_{NL}[f,f] \rightarrow C_{FP}[f,\langle f \rangle] + P[f] \cdot \langle f \rangle, \tag{10}$$

where <f> is the isotropic part of the distribution function (in the velocity space), $C_{FP}[f,<f>]$ is the full nonlinear Fokker-Plank operator describing collisions with an isotropic background, and P[f] are model restoring terms, providing conservation of particles, momentum and energy. For the case where <f> is a Maxwellian distribution, the nonlinear collision model reduces to the linearized collision model. Implementation of the nonlinear collision model is underway.

4 Conclusion

In the present work we have reported on the implementation and testing of a succession of increasingly detailed collision operator options, including a simple drag-diffusion operator in parallel velocity space, Lorentz collisions, and a linearized model Fokker-Planck collision operator conserving momentum and energy. Based on the generalization of the linearized operator we have also formulated a model nonlinear collision operator for the case where a distribution function is nearly isotropic, but arbitrary in speed. We have performed a number of verification tests of these operators, including recovery of analytic results for loss over a prescribed potential barrier and recovery of the neoclassical fluxes.

References

[1] R. H. Cohen and X. Q. Xu, Contrib. Plasma Phys. **48**, 212 (2008).
[2] X. Q. Xu et al., Nucl. Fusion 50, 064003 (2010); Phys. Rev. Lett 100, 215001, (2008).
[3] P. Colella et al., J. Comput. Phys. 230, 2952 (2011).
[4] M. R. Dorr et al., in: Proceedings of the SciDAC 2010 Conference, Tennessee 2010.
[5] P. Colella and M. D. Sekora, J. Comput. Phys. **227**, 7069 (2008).
[6] T. S. Hahm, Phys. Plasmas **3**, 4658 (1996).
[7] X. Q. Xu et al., Nucl. Fusion **47**, 809 (2007).
[8] I. G. Abel et al, Phys. Plasmas **15**, 122509 (2008).
[9] T. D. Rognlien and T. A. Cutler, Nucl. Fusion 20, 1003 (1980).
[10] S. Z. Lin, W. M. Tang, and W. W. Lee, Phys. Plasmas **2**, 2975 (1995).